The Asymmetric Influence of the Two Types of El Niño and La Niña on Summer Rainfall over Southeast China

MUHAMMAD AFZAAL KARORI

State Key Laboratory of Numerical Modeling for Atmospheric Sciences and Geophysical Fluid Dynamics, Institute of Atmospheric Physics, Chinese Academy of Sciences, Beijing, China, and Pakistan Meteorological Department, Islamabad, Pakistan

JIANPING LI

State Key Laboratory of Numerical Modeling for Atmospheric Sciences and Geophysical Fluid Dynamics, Institute of Atmospheric Physics, Chinese Academy of Sciences, Beijing, China

FEI-FEI JIN

Department of Meteorology, School of Ocean and Earth Science and Technology, University of Hawaii at Manoa, Honolulu, Hawaii

(Manuscript received 17 May 2012, in final form 11 December 2012)

ABSTRACT

In this study, the authors demonstrate that the two types of El Niño–Southern Oscillation (ENSO) have asymmetric features with respect to the impact of their positive and negative phases on boreal summer rainfall over the Yangtze River Valley (YRV) and South China (SC). The relationship between rainfall over the YRV and the warm pool (WP) La Niña is positive and significant, whereas the relationship with the WP El Niño is not. In the case of the cold tongue (CT) ENSO, its positive phase has a positive influence, while there is no significant relationship with the negative phase. In contrast, rainfall over SC has a significant positive relationship with WP El Niño, but a nonsignificant relationship with WP La Niña. The positive phase of the CT ENSO has a significant negative influence on SC rainfall, while the negative phase has a nonsignificant impact. An asymmetric atmospheric response to the asymmetric sea surface temperature anomalies (SSTAs) was also observed in the lower troposphere. The location of the center of the anomalous circulations over the study region differs during the opposite phases of the two types of ENSO. This asymmetric response is likely to be linked to the different spatial patterns of the two types of El Niño and La Niña. Atmospheric general circulation models confirm the authors' analysis of the observed data. Numerical simulations show that the asymmetric response of the lower atmosphere is driven mainly by differing SSTA patterns in the equatorial Pacific Ocean.

1. Introduction

El Niño–Southern Oscillation (ENSO) has a significant impact on seasonal climate around the globe. This phenomenon, which develops in the Pacific Ocean, generates significant anomalous patterns in regional and global climate (e.g., Ropelewski and Halpert 1987, 1996; Huang and Wu 1989; Harrison and Larkin 1998; Smith et al. 1999; Trenberth and Caron 2000). ENSO is a very important part of seasonal forecasting because of its influence on climate variability. However, this influence is highly sensitive to changes in the location of the warm anomaly center, that is, changes in the ENSO regime (Ren and Jin 2011). Thus, the outcome of each event may not be exactly the same (Weng et al. 2007). It has been established that climate variations over East Asia are related to the ENSO cycle, and this is attributed to the development of an anomalous anticyclone over the western North Pacific (WNP) during the conventional El Niño,

Corresponding author address: Dr. Jianping Li, Deputy Director and Professor, State Key Laboratory of Atmospheric Sciences and Geophysical Fluid Dynamics (LASG), Institute of Atmospheric Physics, Chinese Academy of Sciences, P.O. Box 9804, Beijing 100029, China.
E-mail: ljp@lasg.iap.ac.cn

DOI: 10.1175/JCLI-D-12-00324.1

also known as a cold tongue (CT) El Niño (e.g., Huang and Wu 1989; Wang et al. 1999, 2000; Wu et al. 2009; Ding et al. 2010; Li et al. 2010, 2011a,b; Wu et al. 2012). It has been shown that, during the boreal summer following the mature phase of a CT El Niño, a positive rainfall anomaly occurs over the Yangtze River Valley (YRV), while a negative rainfall anomaly develops over southern and northern China (Zhang et al. 1999; Feng and Hu 2004; Xue and Liu 2008; Li et al. 2011a,b), linked to the WNP anticyclone. Development of this anomalous anticyclone is attributed to local air–sea interactions and the remote impacts of the Indian Ocean (Watanabe and Jin 2002; Yang et al. 2007; Xie et al. 2009). The influence of the Indian Ocean dipole (IOD) (Behera et al. 1999; Saji et al. 1999; Webster et al. 1999) on ENSO events and their combined effect on atmospheric circulation has also been studied previously (Ashok et al. 2001, 2004; Yu et al. 2002; Saji and Yamagata 2003).

Recent studies have revealed a new variant of the El Niño phenomenon, which is referred to as the warm pool (WP) El Niño (Kug et al. 2009). The WP El Niño is also known as the date line El Niño (Larkin and Harrison 2005), El Niño Modoki (Ashok et al. 2007), or the central Pacific El Niño (Yu and Kao 2007; Kao and Yu 2009). The spatial patterns, dynamics, and evolution of this new type of ENSO have been discussed in detail in earlier studies (e.g., Ashok et al. 2007; Kao and Yu 2009; Kug et al. 2009; Yeh et al. 2009; Yu et al. 2010; Yu and Kim 2010, 2011; Kug and Ham 2011). The WP El Niño has become more frequent over recent decades and has an influence on seasonal climate (Ashok et al. 2007; Kao and Yu 2009; Kug et al. 2009; Yeh et al. 2009; Zhang et al. 2012). Yeh et al. (2009) calculated the frequency of WP and CT ENSO events using the Hadley Centre Sea Ice and Sea Surface Temperature (HadISST) dataset (Rayner et al. 2003) for the period between 1870 and 2007. They found that the frequency, in terms of the occurrence ratio, of the WP El Niño (CT El Niño) before and after 1990 is 0.05 yr^{-1} (0.21 yr^{-1}) and 0.41 yr^{-1} (0.11 yr^{-1}), respectively.

The climatic impacts of the WP El Niño differ from those of the CT El Niño. For example, seasonal weather anomalies over the United States associated with WP and CT El Niños differ substantially from each other in amplitude, spatial coverage, and sign (Larkin and Harrison 2005). Weng et al. (2007) identified the differing impacts of the two types of El Niño in the regions surrounding the Pacific Ocean. They observed two midtropospheric wave trains over the North Pacific, which contained the positive phase of the Pacific–Japan pattern over the WNP and a positive phase of Rossby wave train known as the Pacific–North American (PNA) pattern (Horel and Wallace 1981) in the northeastern Pacific during WP El Niño events. Cai and Cowan (2009) showed that the two ENSO variants exhibit strong asymmetry in their influence between La Niña and El Niño on Australian rainfall during the austral autumn and also in other seasons (Cai and van Rensch 2012). Cai et al. (2010) also reported the asymmetry of the ENSO Modoki phenomenon and its impacts on Australian rainfall during the austral summer. Weng et al. (2011) studied the individual and combined impact of the IOD, and the WP and CT ENSO on observed station rainfall over China during the months of June–August (JJA). Kim et al. (2009) found differing impacts from the two types of ENSO on Atlantic Ocean hurricanes. Chen (2011) reported that the frequency of tropical cyclones in the South China Sea (SCS) increases during a WP El Niño but decreases during a CT El Niño. Feng et al. (2010) investigated the contrasting impacts of the two types over East Asia through the boreal winter using observed data and numerical simulations based on a simple baroclinic model. Feng and Li (2011) investigated the influence of El Niño Modoki and the conventional El Niño on spring rainfall over South China (SC) and proposed the corresponding mechanisms. They found that anomalous flows are associated with anomalous convergence in the upper troposphere over the western Pacific. An anticyclonic circulation that causes a northeasterly flow over the region influences SC. As a result, convection is suppressed and rainfall is reduced during a WP El Niño. During a CT El Niño, the WNP is under the influence of an anomalous anticyclone that brings southerly warm and moist flows into SC, which increases the rainfall anomaly. Zhang et al. (2011) found that the two types of El Niño have opposite impacts on the WNP atmospheric circulation during the boreal autumn and, thus, on autumn rainfall over SC. Xie et al. (2012) identified signals from El Niño Modoki (Ashok et al. 2007) in the tropical tropopause and stratosphere. They found a contrasting effect from the two types of ENSO in the mid- to high-latitude stratosphere. The studies mentioned above depict the development of a zonally elongated anomalous circulation over the WNP during WP El Niño events related to a westward shift of the warm sea surface temperature anomaly (SSTA) center in the equatorial Pacific.

The response of the tropical atmosphere is well understood as a baroclinic response to the diabatic heating anomalies induced by SSTAs (Gill 1980), the so-called Rossby wave response. The Gill-type response of the atmosphere is confined to the tropical regions. Hoskins and Karoly (1981) found that the response of the lower atmosphere to tropical thermal forcing is mostly confined

to the vicinity of the source, while for midlatitude thermal forcing, the atmospheric response depends on the vertical structure of the source. They also demonstrated that in the lower troposphere the response is confined to the region of the source, but this is not the case in the upper troposphere, where the source generates wave trains that are very similar to the equivalent barotropic Rossby wave trains, and they teleconnect the effect of the tropical thermal forcing (e.g., ENSO) to higher latitudes. In the Northern Hemisphere, the PNA teleconnection pattern (Horel and Wallace 1981) is an example of such a wave train. The impact of this pattern is to modulate storm tracks over the northeastern Pacific and across North America during conventional ENSO events. The equivalent pattern in the Southern Hemisphere, which affects South America, is referred to as the Pacific–South American (PSA) pattern (Karoly 1989; Ghil and Mo 1991; Cai et al. 2011).

In this study, we examine the asymmetric impacts of the positive and negative phases of the two types of ENSO on rainfall over the YRV and SC during the boreal summer. Most of the previous studies mentioned above (e.g., Weng et al. 2007, 2011; Feng et al. 2010; Zhang et al. 2011) assume that the impacts of the positive and negative phases of the two ENSO variants are symmetrical. We also show here that an asymmetry exists in the SSTAs during the positive and negative phases of the WP and CT ENSO events and in the associated circulation anomalies that influence rainfall in the study area during the boreal summer.

The study area is an important economic zone and densely populated. Rainfall variability in this region during the boreal summer has a significant impact upon the daily lives of the inhabitants and also on economic growth. Flooding along the Yangtze River can result in a heavy loss of life and property and have a detrimental impact on the economy. This study aims to develop an improved understanding of the underlying mechanisms that govern this kind of climatic phenomena and improve the skill of seasonal prediction for the region, which would help to mitigate the adverse effects of climate-related disasters. Therefore, we focus on the WNP atmospheric circulation associated with the WP and CT ENSO events in an attempt to explain the mechanism by which these events influence the study region. The remainder of the manuscript is organized as follows. Section 2 describes the data and methods used in the study, and section 3 outlines the asymmetrical nature of the relationship between rainfall and the positive and negative phases of the WP and CT ENSO events during JJA. Section 4 describes the asymmetry in the SSTAs and associated circulation anomalies during these same events, and finally, a summary and discussion are presented in section 5.

2. Data, methodology, and model experiment

a. Data and methodology

We use several data sources that focus on the boreal summer over the period between 1979 and 2011: global SST data from HadISST with a resolution of $1° \times 1°$ (Rayner et al. 2003); atmospheric data from the National Centers for Environmental Prediction–National Center for Atmospheric Research (NCEP–NCAR) reanalysis (Kalnay et al. 1996); 160-station monthly mean rainfall data from the China Meteorological Administration; the Global Precipitation Climatology Project (GPCP), version 2.2 (Adler et al. 2003), precipitation dataset (used to verify our results); and the interpolated outgoing longwave radiation (OLR) dataset (Liebmann and Smith 1996). Both the OLR and GPCP datasets were provided by the National Oceanic and Atmospheric Administration, Earth System Research Laboratory, Physical Science Division, Boulder, Colorado, from their website (http://www.esrl.noaa.gov/psd/). The rainfall domain for this study is southeast China (20°–32.5°N, 105°–125°E). This domain has been divided into two subdomains shown in Fig. 1a. The rainfall data were averaged over the region 27.5°–32.5°N, 105°–125°E to determine the rainfall time series of the YRV. The rainfall time series for SC was obtained by taking the average rainfall over the region 20°–27.5°N, 105°–125°E. This study focuses on the period after 1979 to allow the use of satellite data.

Since the discovery of the new form of ENSO event, many indices have been proposed to both characterize it and differentiate it from the conventional ENSO. For example, the WP ENSO index (Kug et al. 2009), the ENSO Modoki index (Ashok et al. 2007), the central Pacific (CP) and eastern Pacific (EP) ENSO indices (Kao and Yu 2009), the CP and EP indices (Yu et al. 2011), and the N_{CT} index for the CT ENSO and the N_{WP} index for the WP ENSO (Ren and Jin 2011). As the studies of the contrasting impacts of the two types of ENSO on the East Asian climate are typically carried out using the ENSO Modoki index (EMI) and Niño-3 index N_3, we also used these indices in this study to avoid any differences that may have arisen because of the use of different indices. Moreover, the choice of these indices is justified by Ashok et al. (2007) and Weng et al. (2007). The empirical orthogonal function (EOF) analysis of the tropical Pacific Ocean SSTA for the period between 1979 and 2011 also supports the use of the EMI and N_3 indices. The spatial patterns of the two leading modes, EOF1 and EOF2, resemble the conventional El Niño and EMI, respectively (figure not shown). The correlation coefficient of the relationship between the first principal component and N_3 is 0.96

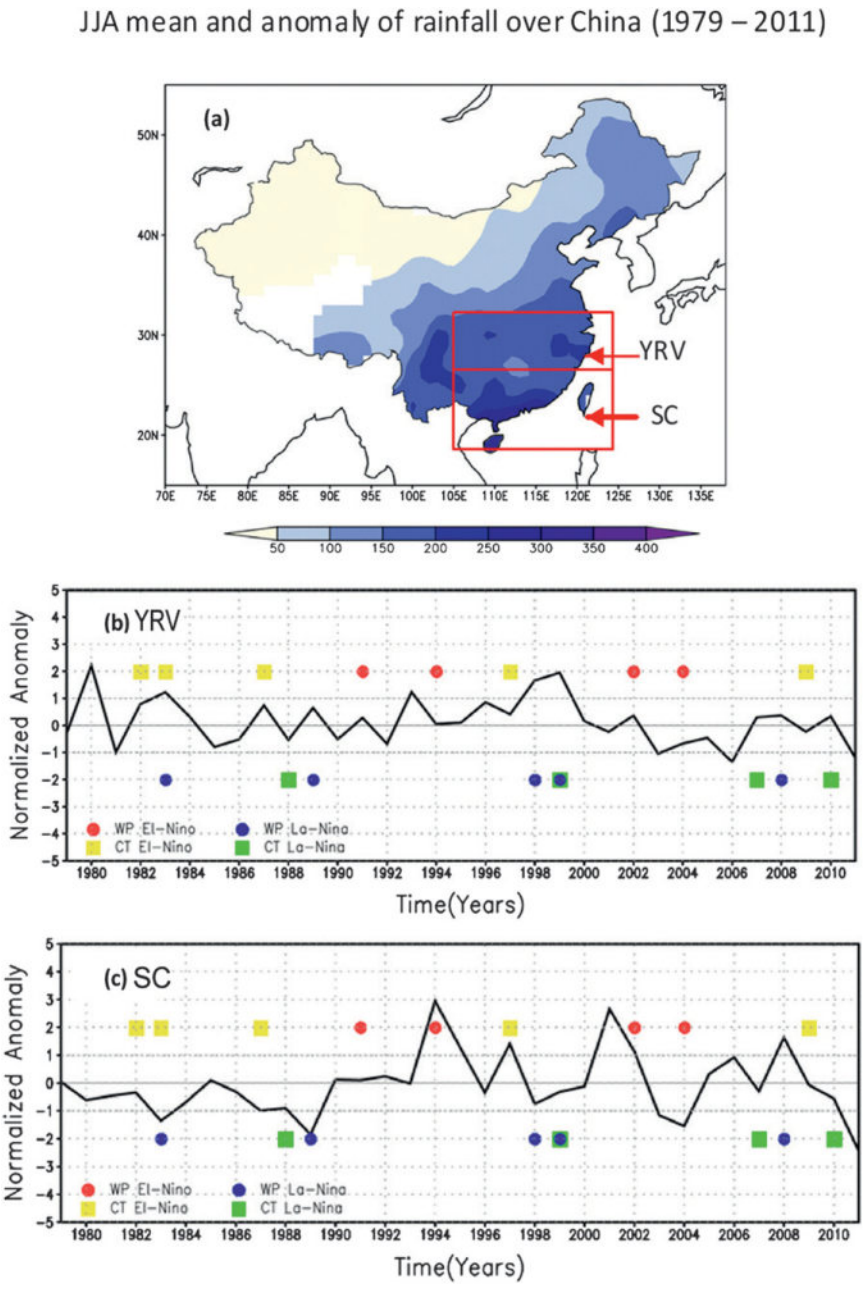

FIG. 1. (a) Spatial distribution of JJA-mean rainfall over China based on station data (mm month^{-1}) for YRV and SC. (b) The time series of JJA normalized rainfall anomaly obtained by taking the area average over YRV. (c) As in (b), but for SC. Red (blue) dots represent the WP El Niño (WP La Niña) and yellow (green) squares are for CT El Niño (CT La Niña) events. The broken line is the one std dev of respective variables.

and between the second principal component and EMI is 0.98.

According to Ashok et al. (2007), the EMI is defined as

$$\mathrm{EMI} = [\mathrm{SSTA}]_{\mathrm{C}} - \frac{1}{2}\{[\mathrm{SSTA}]_{\mathrm{E}} + [\mathrm{SSTA}]_{\mathrm{W}}\},$$

where the square brackets with a subscript represent the SSTA averaged over a central region (C: 10°S–10°N, 165°–140°W), an eastern region (E: 15°S–5°N, 110°–70°W), and a western region (W: 10°S–20°N, 125°–145°E) (available at http://www.jamstec.go.jp/frcgc/research/d1/iod/modoki_home.html.en). The CT ENSO has been quantified by the N_3 index, which is the average of the

TABLE 1. WP ENSO and CT ENSO years, based on ± one std dev of JJA-mean SSTAs for the period 1979–2011.

EMI		Niño 3	
WP El Niño	WP La Niña	CT El Niño	CT La Niña
1991	1983	1982	1988
1994	1989	1987	1999
2002	1998	1997	2007
2004	2008	2009	2010

SSTA over the region (5°S–5°N, 150°–90°W) (available at http://www.cpc.noaa.gov/data/indices/).

Linear regression analysis was used in this study to determine the influence of the positive and negative phases of the WP and CT ENSO events and was applied separately to the positive and negative index years. Normalized time series of the predictor and predictand were used to generate comparably sized regression anomalies. Partial regression/correlation between predictor and predictand has also been applied to remove the effect of other phenomena.

Composite analysis was also used to check the robustness of our results and to separate the symmetric and asymmetric components of the SSTA during the two types of ENSO event. The difference between the composite El Niño and La Niña was taken as a symmetric component, while the difference between the opposite El Niño (i.e., El Niño SSTA × −1) and La Niña was taken as an asymmetric component (Hoerling et al. 1997). Composite anomalies were obtained for the years in which the WP and CT ENSO index was one standard deviation higher/lower than the mean value during the study period. Following the criteria of one standard deviation, the list of both types of ENSO years is given in Table 1, and the monthly means from June, July, and August of each year (Table 1) were used to calculate the composite-mean anomalies. The significance of the regression coefficient and composite anomalies was calculated using a two-tailed Student's *t* test. All datasets used were linearly detrended to allow a focus on interannual variability. To test the hypothesis that the asymmetric influence of the positive and negative phases of the two types of ENSO event is because of different SSTA patterns, we conducted a set of numerical experiments using an atmospheric general circulation model (AGCM).

b. Model description and experimental design

The AGCM used in this study was the Community Atmosphere Model, version 3.1 (CAM3.1), which was developed by NCAR (http://www.ccsm.ucar.edu/models/atm-cam/). A general overview of the model is given by Collins et al. (2004, 2006). The model was run at a horizontal resolution roughly equivalent to 2.8° latitude × 2.8° longitude, with 26 vertical levels in a hybrid sigma-pressure coordinate system that extended from the surface to 4 hPa. The observational SST data, used as the lower boundary condition, are monthly climatologies for the period 1949–2001 (Rayner et al. 2003). We designed seven sensitivity experiments with different boundary conditions (Table 2). Composite-mean SSTs for opposite phases of the two ENSO variants were added to the climatological SST field to create SST forcing for the corresponding experiment. Twenty time-slice runs were performed for each experiment. Ensemble-mean anomalies for JJA were calculated as the departure from the control run.

3. Asymmetric relationship with JJA rainfall

Spatial distribution of JJA-mean rainfall over China is shown in Fig. 1a. Figures 1b and 1c highlight the conjunction of dry and wet boreal summers over the YRV and SC, with extreme positive and negative phases of the indices between 1979 and 2011. Area-averaged rainfall amounts over the YRV were normal in three out of four WP El Niño events. During 2004, the rainfall was below normal but within one standard deviation (Fig. 1b). This indicates a weak relationship between the positive phase of the WP ENSO and rainfall over the YRV. During the negative phase of the WP ENSO, the rainfall anomaly was well above normal in three out of five WP La Niña events, and in two events the rainfall anomaly was positive, within one standard deviation. This indicates positive impact of the WP La Niña on JJA rainfall

TABLE 2. List of numerical experiments: control run (CTRL), WP El Niño run (WPE), Opposite WP El Niño run (ANTWPE), CT El Niño run (CTE), Opposite CT El Niño run (ANTCTE), WP La Niña run (WPLA), and CT La Niña run (CTLA).

Experiment	SST forcing field	Integration (realizations)
CTRL	Global climatological SST	20
WPE	Added composite positive SSTA to climatological SST over 20°S–20°N, 165°E–140°W	20
ANTWPE	Added WPE SSTA multiplied by −1 to climatological SST over 20°S–20°N, 165°E–140°W	20
CTE	Added composite positive SSTA to climatological SST over 10°S–10°N, 180°–80°W	20
ANTCTE	Added CTE SSTA multiplied by −1 to climatological SST over 10°S–10°N, 180°–80°W	20
WPLA	Added composite negative SSTA to climatological SST over 20°S–20°N, 165°E–140°W	20
CTLA	Added composite negative SSTA to climatological SST over 10°S–10°N, 180°–80°W	20

in the region. The rainfall anomaly over the YRV was well above normal in three out of four CT El Niño events. The rainfall anomaly in 1997 was 0.4 of one standard deviation. The rainfall anomaly was normal in two out of three CT La Niña events. This might be because of the weak relationship between the negative phase of the CT ENSO and rainfall. A significant positive anomaly occurred during the 1999 CT La Niña event, which may have been caused by the modulation of the positive influence of the WP La Niña. During 1999, the negative phase of both types of ENSO was observed simultaneously.

Figure 1c shows the JJA rainfall time series from SC over the study period. The highest maximum rainfall anomaly over SC during the study period occurred in conjunction with the positive phase of the WP ENSO in 1994. There were three dry summers in four CT El Niño years. This might be because of the significant negative influence of the CT El Niño. The rainfall anomaly was positive in 1997. An example of the combined influence of a CT El Niño and a WP La Niña on rainfall in both the YRV and SC can be seen in 1983, when both phenomena were observed. Their superimposing effect contributed to flooding in the YRV and drought in SC. These examples, from the years 1994 and 1983, are the same as those pointed out by Weng et al. (2011).

To highlight the asymmetry in the relationship between JJA rainfall and the opposite phases of the two types of ENSO, we calculated lines of best fit for the positive and negative phases of the corresponding ENSO variant. Scatterplots of the normalized precipitation anomaly against N_3 and EMI are shown in Fig. 2. This approach has been used previously in other regions influenced by ENSO (Cai and Cowan 2009). A linear relationship does not exist in either of the scatterplots. For positive values of the indices, the correlation coefficient of rainfall over the YRV with the WP El Niño index is 0.07 and that with the CT El Niño is 0.39 (if the exceptional case of the CT El Niño in 1997 is removed). The correlations of the YRV rainfall with the negative phase of the WP and CT ENSO events are −0.57 and −0.06, respectively (Figs. 2a,b). There is also a significant positive relationship between the YRV rainfall and the CT El Niño, as far as area-averaged JJA rainfall is concerned. This type of nonlinearity has also been observed in previous studies from Australia during different seasons (Cai et al. 2010; Cai and van Rensch 2012). The sensitivity to the WP La Niña is expressed as an increase in rainfall by 0.66 ± 0.23 of one standard deviation per season per one standard deviation decrease in EMI. The sensitivity of the YRV summer rainfall to the CT El Niño is also seen as an increase in rainfall by 0.65 ± 0.45 of one standard deviation per season per one standard deviation increase in N_3. This means that summer season rainfall over the YRV is above average during WP La Niña events, but average to above average during CT El Niño events. In the case of SC, there is a significant positive correlation (0.53) between rainfall and the WP El Niño, while a significant negative correlation (−0.65) exists with the CT El Niño, if the exceptional case of 1997 is removed (Figs. 2c,d). The sensitivity of SC summer rainfall to the WP El Niño is seen as an increase in rainfall of 1.11 ± 0.44 of one standard deviation per season per one standard deviation increase in EMI. The sensitivity of SC summer rainfall to the CT El Niño is represented by a decrease in rainfall of 0.83 ± 0.28 of one standard deviation per season per one standard deviation increase in N_3. The correlation coefficients between JJA rainfall over SC and the YRV with the two types of ENSO for the whole study period, excluding the exceptional year of 1997, are given in Table 3. It can be seen that a significant positive correlation exists between SC rainfall and the WP ENSO, but that the relationship with the CT ENSO is not significant. It can also be observed that there is a significant negative correlation of the YRV summer rainfall with the WP ENSO and a significant positive correlation with the CT ENSO.

The asymmetric effect of the two types of ENSO is also apparent in the horizontal distribution of regression coefficients of rainfall with respect to WP/CT El Niño and WP/CT La Niña in Fig. 3. During a WP El Niño, the rainfall anomaly is negative (positive) over the YRV (SC) (Fig. 3a). There is a positive anomaly over the YRV during a WP La Niña, and no significant anomaly over SC (Fig. 3b). In the case of a CT El Niño, the rainfall is above (below) normal over the YRV (SC). However, below-normal rainfall is not significant over SC (Fig. 3c). In the case of a CT La Niña, there is no significant signal from either the YRV or SC (Fig. 3d). The polarity of the rainfall anomaly is the same over the whole region during a WP La Niña and a CT El Niño. This suggests that the atmospheric response might be similar in a WP La Niña and a CT El Niño, but opposite in a WP El Niño. The signal generated over the region during a CT La Niña is not significant.

The same analysis was carried out on the GPCP dataset, and this yielded the same anomaly patterns over China (figure not shown). It also revealed asymmetric rainfall anomalies in other parts of the world. For example, there is a significant negative anomaly of boreal summer rainfall over southwestern Japan and South Korea during a WP El Niño. The significant positive anomaly shifts toward the east during a WP La Niña. There is a significant negative (positive) anomaly over the western (northwestern) United States during a WP

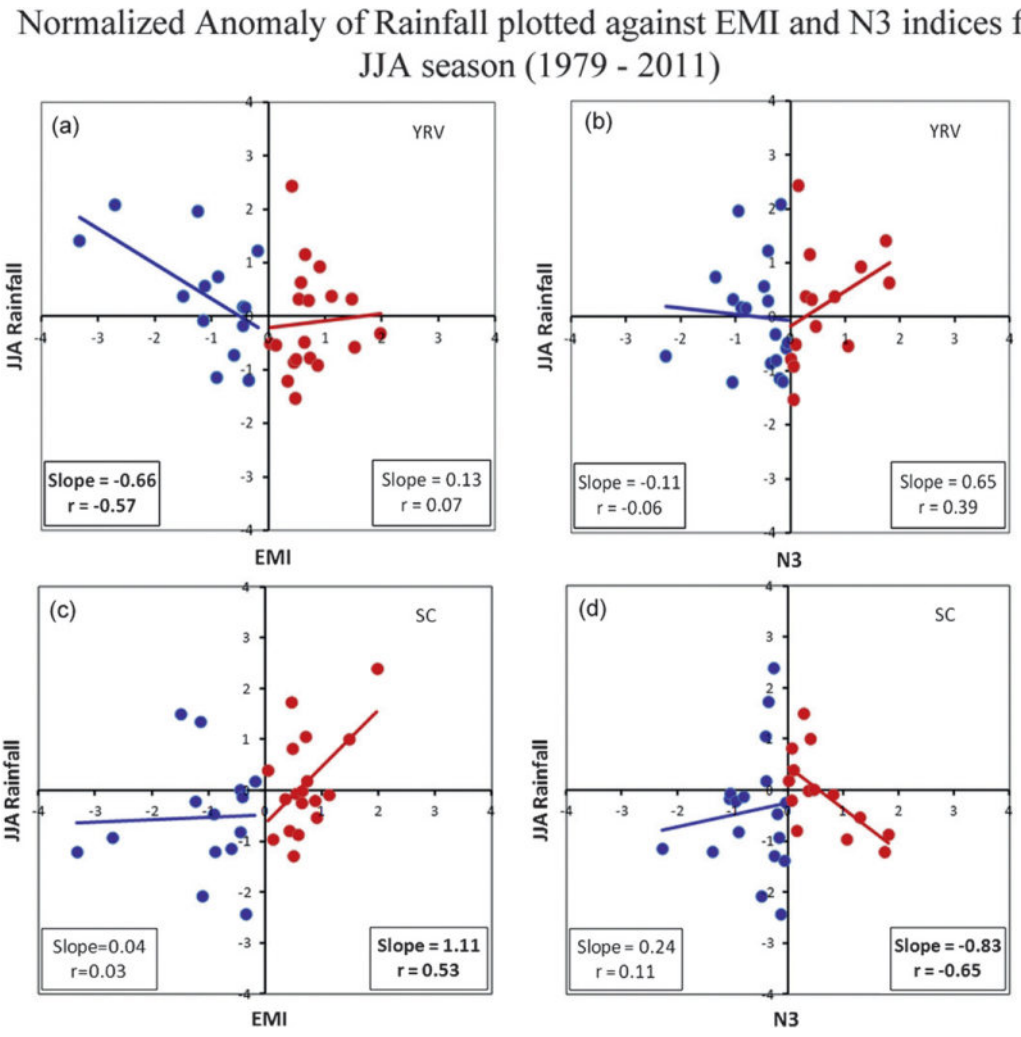

FIG. 2. Normalized JJA rainfall anomaly over YRV plotted against (a) EMI and (b) the N_3 index. (c),(d) As in (a) and (b), but for SC. Lines of best fit for positive and negative EMI/N_3 index values and correlation coefficients (i.e., r) are also shown. The values of the correlation coefficient given in boldface are significant at the 95% level for a two-tailed Student's t test.

El Niño (WP La Niña). A significant asymmetry exists over central northern (southwestern) Australia between the positive and negative phases of the WP ENSO (CT ENSO). The rainfall anomaly patterns associated with WP/CT El Niño events over China, Japan, and the United States are similar to those discussed by Weng et al. (2007) for the boreal summer season. They found that the western North Pacific summer monsoon during a WP El Niño (CT El Niño) is likely to be stronger (weaker) than normal. Wang et al. (2001) also showed that the phases of the summer monsoons in the western North Pacific and East Asia are essentially opposite on an interannual time scale. Therefore, the East Asian summer monsoon in a WP El Niño (CT El Niño) year is likely to be weaker (stronger) than normal. Thus, in a WP El Niño year, SC, the SCS, the Philippines, the Indo-China peninsula, and the western coast of Myanmar are more likely to be wet because of an enhanced western North Pacific summer monsoon, while the YRV, South Korea, and southwestern Japan are more likely to suffer

TABLE 3. Correlation coefficients of the two types of ENSO with rainfall during JJA for the period 1979–2011. Significant coefficients are given in boldface. Confidence level, based on a two-tailed Student's t test, is given in parentheses. The correlations are detrended correlations.

	Yangtze River Valley	South China
WP ENSO	−**0.38** (95%)	**0.31** (90%)
CT ENSO	0.18	0.17

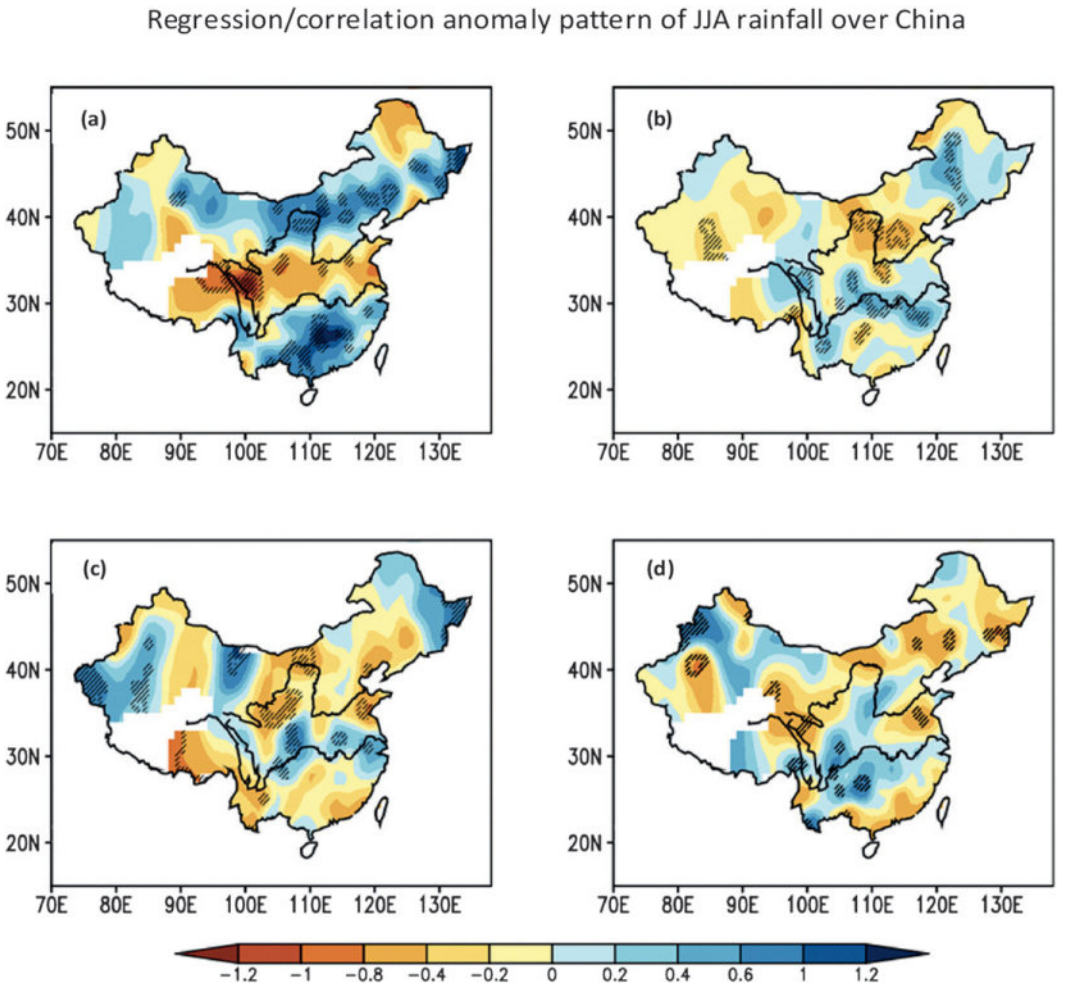

FIG. 3. Normalized regression/correlation anomaly pattern of JJA rainfall over China for (a) WP El Niño events, (b) WP La Niña events, (c) CT El Niño events, and (d) CT La Niña events. Hatched regions indicate regression coefficients significant above the 90% confidence level.

from drought because of the weakened East Asian summer monsoon.

Extreme dry or wet events were also recorded over the study period during neutral ENSO years. This indicates that there are factors other than ENSO that contribute to rainfall anomalies over the study region.

4. Circulation anomalies in WP and CT ENSO and their impacts

a. Climatological mean

The boreal summer climatology of several variables is shown in Fig. 4 to allow a comparison of the difference between the WP and CT ENSO years given in section 4c. Figure 4a shows the JJA-average OLR and streamfunction ψ at 850 hPa. Anticyclonic circulation can be seen over the North Pacific Ocean. The study area lies at the western edge of this anticyclonic circulation. There is a cyclonic circulation over the Bay of Bengal. The combined effect of these circulations is that they bring warm and moist southerly winds from the SCS into the study region, and this causes summer precipitation. The OLR anomalies represent the climatology of the main convection zones (Fig. 4a). The mean position of the subtropical high in the North Pacific is around 30° latitude. The zones of suppressed convection can also be seen in the areas under the subtropical high (Fig. 4a). Lower tropospheric–mean winds and precipitation are given in Fig. 4b. Along the convergence centers (Fig. 4a) and tropospheric winds, the main rainband is located over the warm pool of the western Pacific, southeast China, and the Bay of Bengal along the equatorial and eastern Pacific Ocean (Fig. 4b).

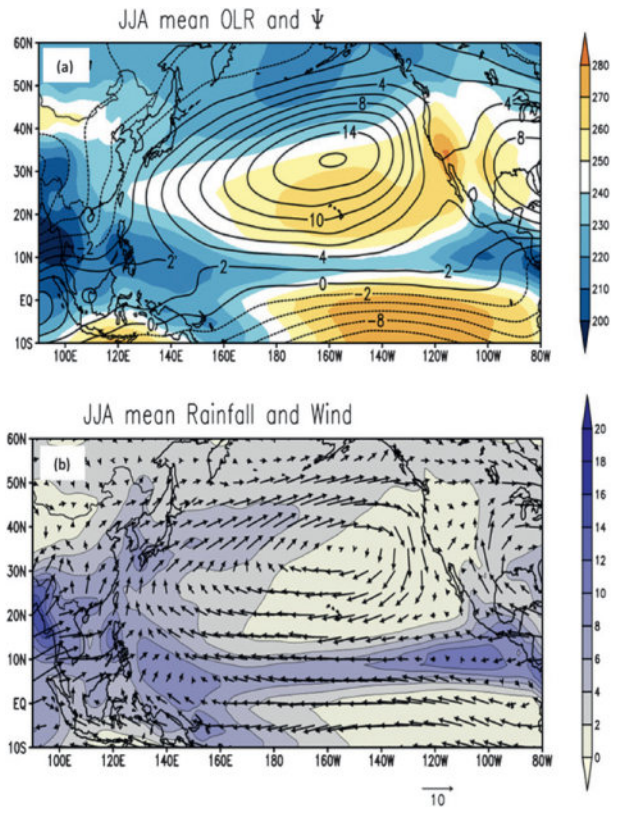

FIG. 4. Boreal summer climatology for the period 1979–2011: (a) OLR (shading; W m^{-2}) and streamfunction at 850 hPa (contours; interval: 2×10^6 m^2 s^{-1}) and (b) GPCP precipitation rate (shading; mm day^{-1}) and wind at 850 hPa (vectors; reference vector provided below panel).

b. *Asymmetry in SSTA patterns*

We used composite analysis to highlight the asymmetry in the SSTA associated with the WP and CT ENSO events during JJA. Figure 5 shows the composite-mean SSTA, and the difference in the composite means between the positive and negative phase of the two types of ENSO. The composite-mean SSTAs from WP El Niño and La Niña events are shown in Figs. 5a and 5b and from CT El Niño and La Niña events in Figs. 5c and 5d, respectively. The patterns are similar to the well-known WP and CT El Niños discussed in earlier studies (Ashok et al. 2007; Weng et al. 2007, 2011). Figures 5e and 5g show the symmetric components of the two types of the El Niño patterns. Figure 5i demonstrates the asymmetry between the SSTA in a positive phase of the two types of El Niño and shows that significant asymmetry exists over the central-eastern tropical Pacific, with a maximum over the far eastern Pacific. The asymmetry in atmospheric circulation anomalies over the WNP and eastern Asia is caused by the asymmetric SSTA pattern in the tropical Pacific during the two types of El Niño (e.g., Weng et al. 2007, 2011; Feng and Li 2011; Zhang et al. 2011).

The SSTAs over the tropical Pacific are also asymmetric features in the positive and negative phase of both types of ENSO event. Figures 5f and 5h show the asymmetric components of the two types of ENSO, and there is a significant asymmetry between the WP El Niño and La Niña in the far eastern tropical Pacific and the tropical northeastern Pacific (Fig. 5f). This suggests that the positive SSTAs during a WP La Niña in the tropical eastern Pacific are stronger than the negative SSTAs during a WP El Niño. There are small-scale regions of significant asymmetry in the central tropical Pacific, where the negative SSTAs during the WP La Niña are weaker than the positive SSTAs during the WP El Niño. Similarly, Fig. 5h shows the asymmetric SSTAs during the CT El Niño and La Niña. The negative SSTAs during the CT La Niña are weaker (stronger) than the positive SSTAs during the CT El Niño in the eastern (central) tropical Pacific. The asymmetry in the CT El Niño and La Niña during JJA is little different to previous studies (e.g., Wu et al. 2010). Wu et al. (2010) pointed out that SSTAs during JJA are generally symmetric for the CT El Niño and La Niña, but the SSTA tendency is asymmetric because of the highly asymmetric latent heat flux anomalies at that time. However, our results for JJA show significant asymmetric regions of SSTA in the tropical Pacific. It is important to determine whether this asymmetry only emerged in recent years.

The asymmetric SSTAs in the tropical Pacific have also been observed during the two types of La Niña (Fig. 5j). The positive SSTAs during a WP La Niña is stronger than the negative anomaly during a CT La Niña in the far eastern tropical Pacific. The SSTA sign is the same in the central and western tropical Pacific during both La Niña variants, but the anomaly is stronger during a CT La Niña. The asymmetry pattern is generally similar to the typical CT La Niña pattern. Previous studies indicate that the two types of La Niña are less distinguishable (e.g., Kug et al. 2009, 2010; Kug and Ham 2011) during their peak phase, that is, the boreal winter. Our results from JJA also show that there is a similar SSTA pattern over most of the tropical Pacific during the two types of La Niña. However, there is a strong asymmetry in the far eastern tropical Pacific.

The above results imply that there is an asymmetry in SSTAs during the opposite phases of the two types of ENSO, and we believe that it is very important for the causes of this asymmetry, and the nature of its evolution during the different phases, to be determined. However, these questions are beyond the scope of this study. In the next section we discuss whether or not the

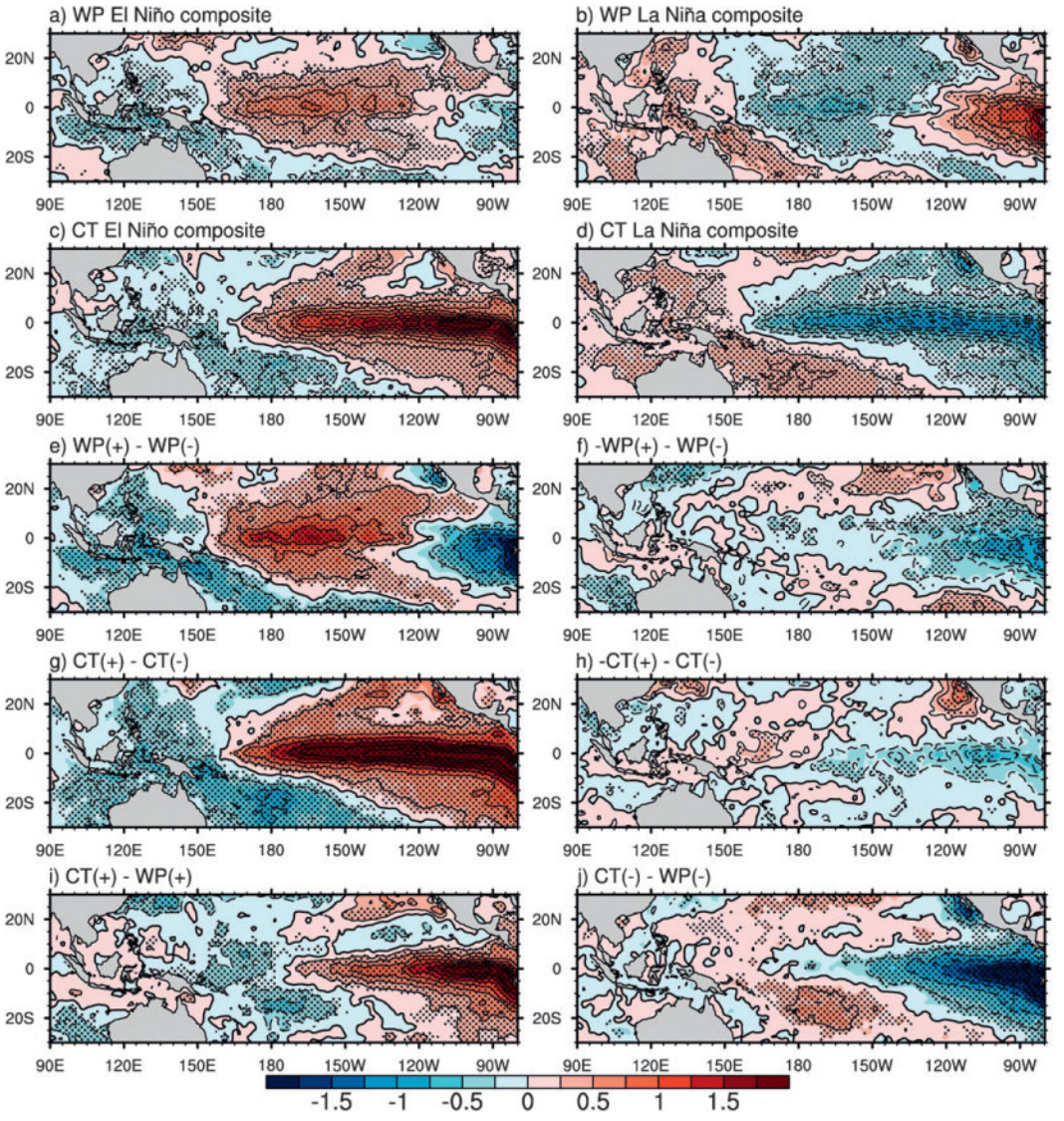

FIG. 5. Composite-mean SSTAs in JJA: (a) WP El Niño, (b) WP La Niña, (c) CT El Niño, and (d) CT La Niña. Composite-mean SST difference between (e) WP El Niño and WP La Niña, (f) opposite WP El Niño and WP La Niña, (g) CT El Niño and CT La Niña, (h) opposite CT El Niño and CT La Niña, (i) CT El Niño and WP El Niño, and (j) CT La Niña and WP La Niña. The stippled regions represent the 10% significance level.

atmospheric response to different SSTAs in the tropical Pacific is asymmetric and how it influences rainfall over the study region.

c. *Atmospheric circulation anomalies*

The warming in the eastern Pacific induces suppressed convection in the western Pacific and also influences the climate of eastern Asia (e.g., Huang and Wu 1989; Zhang et al. 1996; Wang et al. 2000; Wu et al. 2009; Ding et al. 2010; Li et al. 2010, 2011a,b; Wu et al. 2012). This influence is mainly attributed to the development of an anomalous anticyclone over the WNP. During the CT El Niño, there is a central Pacific cyclone, western North Pacific anticyclone, and a northeastern Asia cyclone present in the lower atmosphere. This typical atmospheric pattern is referred to as the Pacific–East Asian teleconnection (PEA), or Rossby wave response, to eastern Pacific warming (Wang et al. 2000; Cai et al. 2011).

A contrasting atmospheric Rossby wave response to asymmetric SSTA patterns emerged during the two types of ENSO. In Fig. 6, blue (orange) represents a negative (positive) anomaly of OLR, and contours represent the streamfunction anomaly at 850 hPa. The lower

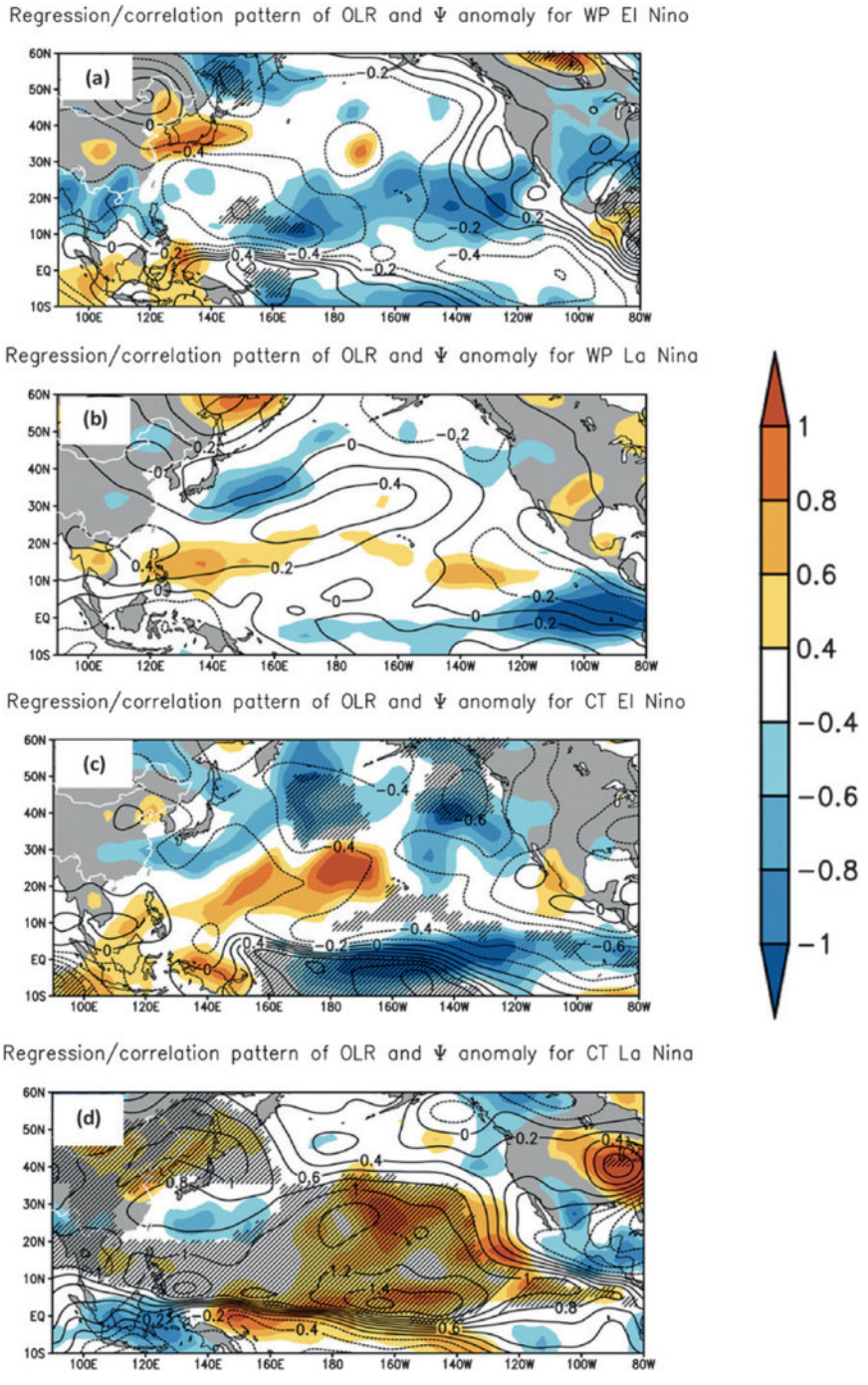

FIG. 6. Normalized regression/correlation anomaly pattern of OLR (shaded) and streamfunction (contours) in JJA for (a) WP El Niño, (b) WP La Niña, (c) CT El Niño, and (d) CT La Niña. Only significant (90% level) OLR anomalies are plotted. Streamfunction anomalies significant at 90% level are hatched.

tropospheric circulations in the WP and CT El Niños (Figs. 6a,c) are similar to those discussed in previous studies (e.g., Wang et al. 2000; Wu and Hu 2003; Weng et al. 2007, 2011; Niu and Li 2008; Feng et al. 2010; Feng and Li 2011; Zhang et al. 2011). In the WP El Niño years, westerly anomalies in the lower troposphere dominate the tropical WNP. The maximum westerly wind anomaly is observed around 140°E. Strong anomalous

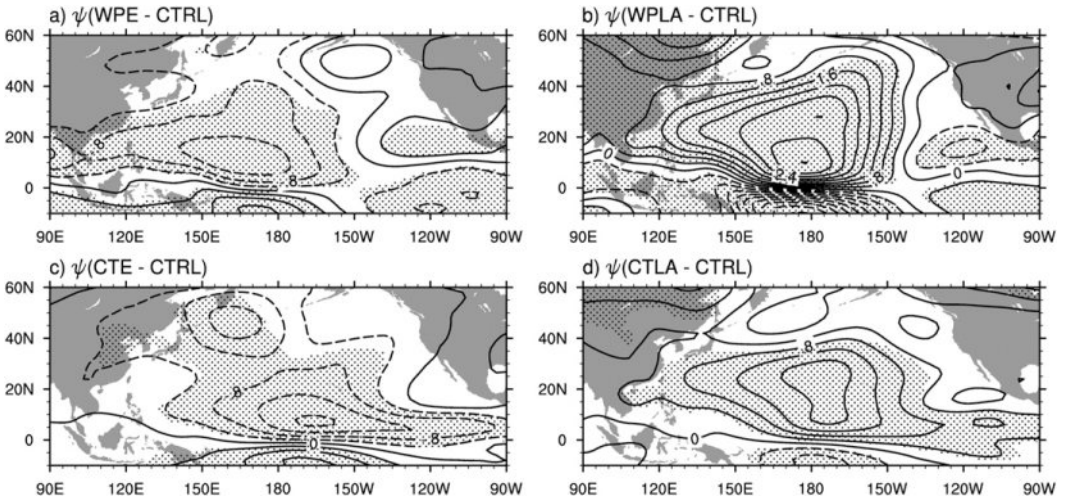

FIG. 7. Simulated 850-hPa streamfunction anomaly (interval: 0.4×10^6 m^2 s^{-1}): (a) WPE minus CTRL runs, (b) WPLA minus CTRL runs, (c) CTE minus CTRL runs, and (d) CTLA minus CTRL runs (see Table 2 for abbreviation explanations). Stippled regions show the significant difference at 95% confidence level.

westerly flows reduce the mean flow over the central Pacific. Because of reduced winds over the sea surface, evaporation is reduced and the SST increases. This warming initiates the cyclonic circulation over the WNP and SCS (Fig. 6a). This kind of air–sea interaction generates a Rossby wave response, or PEA teleconnection, in the lower atmosphere, as described by Wang et al. (2000). Under the influence of the anomalous cyclonic circulation, anomalous easterly flows develop over southeast China that supply moisture to the region. The presence of a deep trough provides an environment conducive to wetter-than-normal summers (i.e., JJA) over SC in the event of a WP El Niño. There is anomalous anticyclonic circulation to the north of 30°N, which may be responsible for the dry monsoon over the northern YRV during the WP El Niño. The WP La Niña enhances the subtropical high that extends westward (Fig. 6b). In the event of a WP La Niña, an anticyclonic circulation exists over the WNP in response to the cooling over the central tropical Pacific. Anomalous easterly winds over the central Pacific enhance the background flows, which reduce the SST, and suppress convection over the central Pacific (Fig. 6b). The warm and moist southerly winds over the northwest flank of the anomalous anticyclone over the SCS converge over the YRV and interact with cold northerly winds. This gives rise to the above-normal rainfall during JJA over the YRV during the WP La Niña. The centers of the anomalous anticyclonic circulation and OLR anomalies are different from their counterparts during a WP El Niño. This asymmetric response of the lower atmosphere and OLR may be linked with the asymmetric SSTAs discussed in the previous section.

During a CT El Niño, the maxima of strong anomalous westerly flow move east with the SSTA center (Fig. 6c). Therefore, an anomalous anticyclonic circulation develops to the northeast of the Philippines. On the western flanks of the anomalous anticyclonic circulation over the WNP, the southerly flows provide moisture to the East Asian region and increase precipitation there. Figure 6c shows a negative OLR anomaly over eastern China and the YRV because of the presence of the WNP anticyclonic circulation and anomalous cyclonic circulation over eastern China and Japan. During a CT La Niña, the anomalous anticyclonic circulation extends westward over the tropical Pacific. The circulations over the WNP are not exactly opposite to those observed during the CT El Niño. The asymmetry between the CT El Niño and La Niña during the boreal winter has been discussed previously (e.g., Hoerling et al. 1997; Wu et al. 2010). Our results for the JJA period also show an asymmetry in the lower atmospheric circulations and OLR anomalies. We analyzed data generated by idealized numerical experiments to confirm the hypothesis that the observed asymmetry in the lower atmospheric circulations is mainly derived from the asymmetric SSTA during opposite phases of the two types of ENSO.

d. Results of numerical experiment

The numerical experiments (Table 2) performed with the AGCM examined asymmetry in lower tropospheric circulations during positive and negative phases of both types of ENSO. The simulated lower tropospheric circulation anomalies are shown in Fig. 7 and can be compared with the 850-hPa streamfunction anomalies shown

in Fig. 6. The broad features of the simulated streamfunction anomalies are similar to the observed anomalies. This may provide evidence that asymmetry in the circulation anomalies is caused by differing SST anomalies during the opposite phases of the two types of ENSO. The model simulated almost inverse streamfunction anomalies when the sign of SST forcing for the WP/CT El Niño was reversed from positive to negative, such as in experiments ANTCTE and ANTWPE (Table 2). The anomaly patterns in this case also differ from the WP and CT La Niña experiments (figure not shown). This further confirms that the asymmetry is derived primarily from different SSTA patterns in opposite phases of the two types of ENSO.

5. Summary and discussion

This study demonstrates the asymmetric influence of the positive and negative phases of WP and CT ENSO events on the YRV and SC boreal summer rainfall. The major findings are summarized below.

During the boreal summer over southeast China, an asymmetrical rainfall anomaly occurs that is associated with the opposite phases of the two types of ENSO. There was a significant positive impact from the WP La Niña on rainfall in the YRV over the study period. This influence remains significant (correlation coefficient = 0.40) over the longer time period of 1951–2011. The WP El Niño had a significant positive impact on rainfall over SC during the study period. In contrast, the CT El Niño had a significant positive (negative) impact on the YRV (SC) rainfall, if the year 1997 is excluded. This relationship is only marginally significant over the longer period. The asymmetry in rainfall anomaly has also been observed over Japan, the United States, Australia, and South Asia. While this paper focuses on southeast China, it may be interesting to investigate the asymmetric impacts of the opposite phases of the two types of ENSO during JJA over these regions as well.

An asymmetry in the SSTA was observed between opposite phases of the individual ENSO variant, and between opposite phases of the two types of ENSO, during the boreal summer. The asymmetric SSTA may be attributed to the asymmetric impact on rainfall over the study region. How the asymmetry in the SSTA emerges and evolves has not been addressed in this study and would be an interesting topic for future research.

An asymmetric atmospheric Rossby wave response to the opposite phases of the two types of ENSO was also observed. An anomalous cyclone over the WNP is the main system during a WP El Niño in the boreal summer. As a Rossby wave response, an anticyclonic circulation appears to the north of 30°N over northeastern China and southern Japan. An anomalous WNP anticyclone appears in response to the cooling over the central equatorial Pacific Ocean during the WP La Niña events. The anomaly centers of OLR and streamfunction associated with WP La Niñas differ from those of their counterparts in a WP El Niño. This asymmetric response is likely to be linked to the asymmetric SSTA patterns during the opposite phases of the WP ENSO events.

There is also an asymmetric response of the lower atmosphere to the positive and negative phases of a CT ENSO. The asymmetric response of the lower atmosphere between a CT El Niño and La Niña, over the WNP (Wu et al. 2010) and over the globe (Hoerling et al. 1997), in the boreal winter has already been discussed. Our results for the boreal summer, based on analysis of the observed and modeled data, also highlight this asymmetry. This asymmetry in the atmospheric response may be linked to the asymmetric SSTA pattern in the CT El Niño and La Niña.

The asymmetry of lower atmospheric circulations over the North Pacific during opposite phases of the two types of ENSO was well simulated by the AGCM forced with idealized warming/cooling in the eastern and central tropical Pacific. This confirms our findings based on the observed circulation patterns. The modeling also showed that the asymmetry in the atmospheric circulations is primarily derived from asymmetric patterns of SSTA during the positive and negative phases of the two types of ENSO. This result agrees with a previous study carried over the boreal winter (Kug and Ham 2011). It would be interesting to investigate the asymmetric impacts of the two types of El Niño and La Niña using a coupled global circulation model.

Figure 8a shows a schematic representation of the Rossby wave response to the positive and negative phases of the WP and CT ENSO events. A lower tropospheric wave initiated from the central Pacific is evident. The moist easterly flows across the northwestern edge of the anomalous cyclone over the WNP during a WP El Niño converge over SC. As a result, SC receives above-normal rainfall while the YRV receives less-than-normal rainfall during a boreal summer WP El Niño. The lower atmospheric circulation setting was similar to previous studies (e.g., Weng et al. 2007, 2011) for JJA. During a WP La Niña, cyclonic circulation over the eastern Pacific develops in response to the warm SST anomaly there. An anomalous anticyclonic circulation develops over the WNP and an anomalous cyclonic circulation develops to the north of 30°N (Fig. 8b), which result in the YRV receiving above-normal rainfall in a WP La Niña year.

For CT El Niño events (Fig. 8c), the anomalous cyclonic/anticyclonic setting was similar to that reported

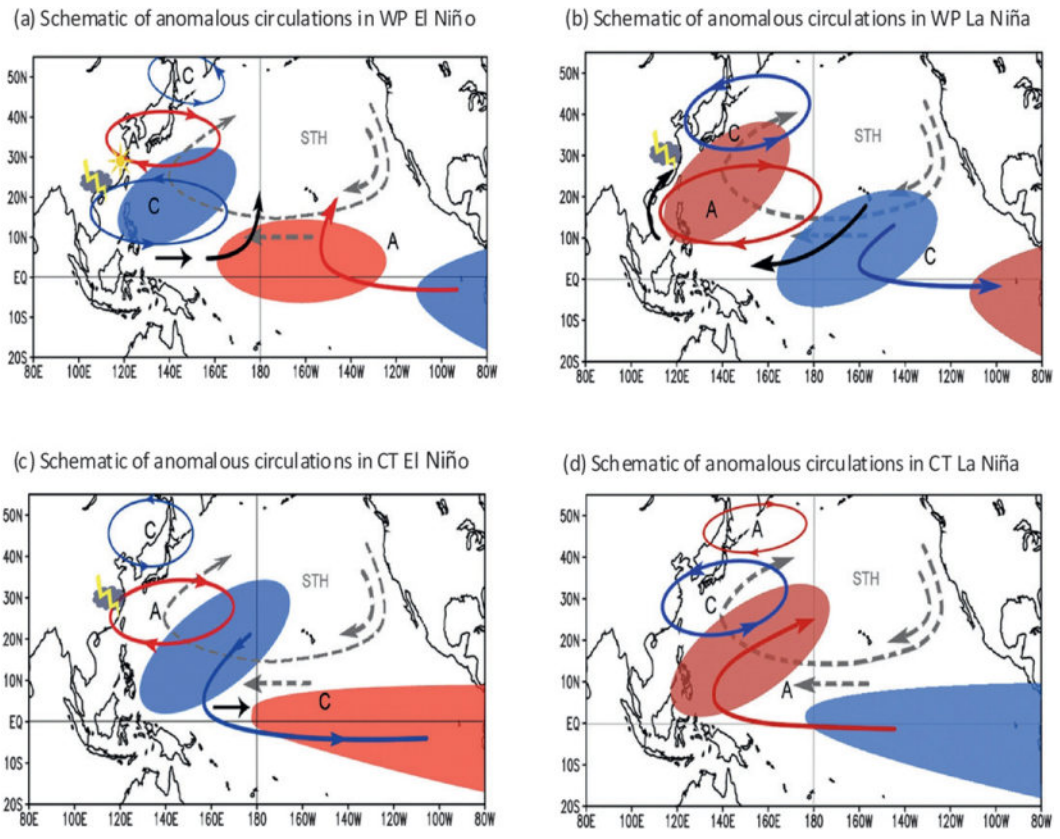

FIG. 8. Schematic representation of the atmospheric circulation anomalies at 850-hPa level associated with (a) WP El Niño, (b) WP La Niña, (c) CT El Niño, and (d) CT La Niña. The areas shaded in red (blue) represent positive (negative) SSTAs. The "STH" is for subtropical high, gray lines show the climatological mean, and black lines show anomalous circulations. The letters "C" and "A" represent cyclonic and anticyclonic circulation, respectively.

in previous studies (Wang et al. 2000; Weng et al. 2007, 2011; Feng et al. 2010; Feng and Li 2011). The WNP anticyclone provides warm and moist southerlies, which, on meeting the cold and dry northerlies, generate above-normal rainfall over the YRV. Figure 8d schematically represents the lower tropospheric circulation during a CT La Niña event, and such CT La Niña events do not have a significant impact on the study region.

The asymmetric features in the impact of the two types of El Niño and La Niña on boreal summer rainfall over southeast China have been demonstrated using observed data and a set of AGCM sensitivity experiments. These asymmetric impacts would be further investigated using coupled general circulation models in future.

Acknowledgments. This work was jointly supported by the 973 Program (2010CB950400), the National Natural Science Foundation of China (41030961), and the CAS Project (XDA5090403). The authors are grateful to three anonymous reviewers for giving valuable suggestions that helped improve the manuscript.

REFERENCES

Adler, R. F., and Coauthors, 2003: The version-2 Global Precipitation Climatology Project (GPCP) Monthly Precipitation Analysis (1979–present). *J. Hydrometeor.,* **4,** 1147–1167.

Ashok, K., Z. Guan, and T. Yamagata, 2001: Impact of the Indian Ocean dipole on the relationship between the Indian monsoon rainfall and ENSO. *Geophys. Res. Lett.,* **28,** 4499–4502.

——, ——, N. H. Saji, and T. Yamagata, 2004: Individual and combined influence of ENSO and the Indian Ocean Dipole on the Indian summer monsoon. *J. Climate,* **17,** 3141–3155.

——, S. K. Behera, S. A. Rao, H. Y. Weng, and T. Yamagata, 2007: El Niño Modoki and its teleconnection. *J. Geophys. Res.,* **112,** C11007, doi:10.1029/2006JC003798.

Behera, S. K., R. Krishnan, and T. Yamagata, 1999: Unusual ocean-atmosphere conditions in the tropical Indian Ocean during 1994. *Geophys. Res. Lett.,* **26,** 3001–3004.

Cai, W., and T. Cowan, 2009: La Niña Modoki impacts Australia autumn rainfall variability. *Geophys. Res. Lett.,* **36,** L12805, doi:10.1029/2009GL037885.

——, and P. van Rensch, 2012: The 2011 southeast Queensland extreme summer rainfall: A confirmation of a negative Pacific Decadal Oscillation phase? *Geophys. Res. Lett.,* **39,** L08702, doi:10.1029/2011GL050820.

——, ——, T. Cowan, and A. Sullivan, 2010: Asymmetry in ENSO teleconnection with regional rainfall, its multidecadal

variability, and impact. *J. Climate,* **23,** 4944–4955, doi:10.1175/2010JCLI3501.1.

——, P. Rensch, T. Cowan, and H. H. Hendon, 2011: Teleconnection pathways of ENSO and the IOD and the mechanisms for impacts on Australian rainfall. *J. Climate,* **24,** 3910–3923.

Chen, G., 2011: How does shifting Pacific Ocean warming modulate on tropical cyclone frequency over the South China Sea? *J. Climate,* **24,** 4695–4700.

Collins, W. D., and Coauthors, 2004: Description of the NCAR Community Atmosphere Model (CAM 3.0). NCAR Tech. Note NCAR/TN-464+STR, 226 pp. [Available online at http://www.cesm.ucar.edu/models/atm-cam/docs/description/description.pdf.]

——, and Coauthors, 2006: The formulation and atmospheric simulation of the Community Atmosphere Model version 3 (CAM3). *J. Climate,* **19,** 2144–2161.

Ding, R. Q., K. J. Ha, and J. P. Li, 2010: Interdecadal shift in the relationship between the East Asian summer monsoon and the tropical Indian Ocean. *Climate Dyn.,* **34,** 1059–1071.

Feng, J., and J. Li, 2011: Influence of El Niño Modoki on spring rainfall over south China. *J. Geophys. Res.,* **116,** D13102, doi:10.1029/2010JD015160.

——, L. Wang, W. Chen, S. K. Fong, and K. C. Leong, 2010: Different impacts of two types of Pacific Ocean warming on Southeast Asian rainfall during boreal winter. *J. Geophys. Res.,* **115,** D24122, doi:10.1029/2010JD014761.

Feng, S., and Q. Hu, 2004: Variations in the teleconnection of ENSO and summer rainfall in northern China: A role of the Indian summer monsoon. *J. Climate,* **17,** 4871–4881.

Ghil, M., and K. C. Mo, 1991: Intraseasonal oscillations in the global atmosphere. Part II: Southern Hemisphere. *J. Atmos. Sci.,* **48,** 780–790.

Gill, A. E., 1980: Some simple solutions for heat-induced tropical circulation. *Quart. J. Roy. Meteor. Soc.,* **106,** 447–462.

Harrison, D. E., and N. K. Larkin, 1998: Seasonal U.S. temperature and precipitation anomalies associated with El Niño: Historical results and comparison with 1997-98. *Geophys. Res. Lett.,* **25,** 3959–3962.

Hoerling, M. P., A. Kumar, and M. Zhong, 1997: El Niño, La Niña, and the nonlinearity of their teleconnections. *J. Climate,* **10,** 1769–1786.

Horel, J. D., and J. M. Wallace, 1981: Planetary-scale atmospheric phenomena associated with the Southern Oscillation. *Mon. Wea. Rev.,* **109,** 813–829.

Hoskins, B. J., and D. J. Karoly, 1981: The steady linear response of a spherical atmosphere to thermal and orographic forcing. *J. Atmos. Sci.,* **38,** 1179–1196.

Huang, R. H., and Y. F. Wu, 1989: The influence of ENSO on the summer climate change in China and its mechanism. *Adv. Atmos. Sci.,* **6,** 21–32.

Kalnay, E., and Coauthors, 1996: The NCEP/NCAR Reanalysis Project. *Bull. Amer. Meteor. Soc.,* **77,** 437–471.

Kao, H. Y., and J. Y. Yu, 2009: Contrasting eastern-Pacific and central-Pacific types of ENSO. *J. Climate,* **22,** 615–632.

Karoly, D. J., 1989: Southern Hemisphere circulation features associated with El Niño–Southern Oscillation events. *J. Climate,* **2,** 1239–1252.

Kim, H.-M., P. J. Webster, and J. A. Curry, 2009: Impact of shifting patterns of Pacific Ocean warming on North Atlantic tropical cyclones. *Science,* **325,** 77–80.

Kug, J. S., and Y. G. Ham, 2011: Are there two types of La Niña? *Geophys. Res. Lett.,* **38,** L16704, doi:10.1029/2011GL048237.

——, F.-F. Jin, and S.-I. An, 2009: Two types of El Niño events: Cold tongue El Niño and warm pool El Niño. *J. Climate,* **22,** 1499–1515.

——, J. Choi, S.-I. An, F.-F. Jin, and A. T. Wittenberg, 2010: Warm pool and cold tongue El Niño events as simulated by the GFDL 2.1 coupled GCM. *J. Climate,* **23,** 1226–1239.

Larkin, N. K., and D. E. Harrison, 2005: On the definition of El Niño and associated seasonal average U.S. weather anomalies. *Geophys. Res. Lett.,* **32,** L13705, doi:10.1029/2005GL022738.

Li, J. P., Z. W. Wu, Z. H. Jiang, and J. H. He, 2010: Can global warming strengthen the East Asian summer monsoon? *J. Climate,* **23,** 6696–6705.

—— , and Coauthors, 2011a: *Ocean–Atmosphere Interaction over the Joining Area of Asia and Indian-Pacific Ocean and Its Impact on the Short-Term Climate Variation in China* (in Chinese). Vol. 1. China Meteorological Press, 516 pp.

——, and Coauthors, 2011b: *Ocean–Atmosphere Interaction over the Joining Area of Asia and Indian-Pacific Ocean and Its Impact on the Short-Term Climate Variation in China* (in Chinese). Vol. 2. China Meteorological Press, 564 pp.

Liebmann, B., and C. A. Smith, 1996: Description of a complete (interpolated) outgoing longwave radiation dataset. *Bull. Amer. Meteor. Soc.,* **77,** 1275–1277.

Niu, N., and J. P. Li, 2008: Interannual variability of autumn precipitation over South China and its relation to atmospheric circulation and SST anomalies. *Adv. Atmos. Sci.,* **25,** 117–125.

Rayner, N. A., D. E. Parker, E. B. Horton, C. K. Folland, L. V. Alexander, D. P. Rowell, E. C. Kent, and A. Kaplan, 2003: Global analyses of sea surface temperature, sea ice, and night marine air temperature since the late nineteenth century. *J. Geophys. Res.,* **108,** 4407, doi:10.1029/2002JD002670.

Ren, H.-L., and F.-F. Jin, 2011: Niño indices for two types of ENSO. *Geophys. Res. Lett.,* **38,** L04704, doi:10.1029/2010GL046031.

Ropelewski, C. F., and M. S. Halpert, 1987: Global and regional scale temperature patterns associated with the El Niño/Southern Oscillation. *Mon. Wea. Rev.,* **115,** 1606–1626.

——, and ——, 1996: Quantifying Southern Oscillation–precipitation relationships. *J. Climate,* **9,** 1043–1059.

Saji, N. H., and T. Yamagata, 2003: Possible impacts of Indian Ocean dipole mode events on global climate. *Climate Res.,* **25,** 151–169.

——, B. N. Goswami, P. N. Vinayachandran, and T. Yamagata, 1999: A dipole mode in the tropical Indian Ocean. *Nature,* **401,** 360–363.

Smith, S. R., D. M. Legler, M. J. Remigio, and J. J. O'Brien, 1999: Comparison of 1997–98 U.S. temperature and precipitation anomalies to historical ENSO warm phases. *J. Climate,* **12,** 3507–3515.

Trenberth, K. E., and J. M. Caron, 2000: The Southern Oscillation revisited: Sea level pressures, surface temperatures, and precipitation. *J. Climate,* **13,** 4358–4365.

Wang, B., R. G. Wu, and X. H. Fu, 2000: Pacific–East Asian teleconnection: How does ENSO affect East Asian climate? *J. Climate,* **13,** 1517–1536.

——, R. Wu, and K. M. Lau, 2001: Interannual variability of the Asian summer monsoon: Contrasts between the Indian and the western North Pacific–East Asian monsoons. *J. Climate,* **14,** 4073–4090.

Wang, C., R. H. Weisberg, and J. I. Virmani, 1999: Western Pacific interannual variability associated with the El Niño-Southern Oscillation. *J. Geophys. Res.,* **104,** 5131–5149.

Watanabe, M., and F.-F. Jin, 2002: Role of Indian Ocean warming in the development of Philippine Sea anticyclone during ENSO. *Geophys. Res. Lett.,* **29,** 1661, doi:10.1029/2001GL014318.

Webster, P. J., A. M. Moore, J. P. Loschnigg, and R. R. Leben, 1999: Coupled ocean-atmosphere dynamics in the Indian Ocean during 1997–98. *Nature,* **401,** 356–360.

Weng, H. Y., K. Ashok, S. K. Behera, S. A. Rao, and T. Yamagata, 2007: Impacts of recent El Niño Modoki on dry/wet conditions in the Pacific rim during boreal summer. *Climate Dyn.,* **29,** 123–129.

——, G. Wu, Y. Liu, S. K. Behera, and T. Yamagata, 2011: Anomalous summer climate in China influenced by the tropical Indo-Pacific Oceans. *Climate Dyn.,* **36,** 769–782.

Wu, B., T. Li, and T. J. Zhou, 2010: Asymmetry of atmospheric circulations over the western North Pacific between El Niño and La Niña. *J. Climate,* **23,** 4807–4822.

Wu, R., and Z. Z. Hu, 2003: Evolution of ENSO-related rainfall anomalies in East Asia. *J. Climate,* **16,** 3742–3758.

Wu, Z. W., B. Wang, J. P. Li, and F.-F. Jin, 2009: An empirical seasonal prediction model of the East Asian summer monsoon using ENSO and NAO. *J. Geophys. Res.,* **114,** D18120, doi:10.1029/2009JD011733.

——, J. P. Li, Z. H. Jiang, J. H. He, and X. Zhu, 2012: Possible effects of the North Atlantic Oscillation on the strengthening relationship between the East Asian summer monsoon and ENSO. *Int. J. Climatol.,* **32,** 794–800, doi:10.1002/joc.2309.

Xie, F., J. P. Li, W. S. Tian, J. Feng, and Y. Huo, 2012: Signals of El Niño Modoki in the tropical tropopause layer and stratosphere. *Atmos. Chem. Phys.,* **12,** 5259–5273, doi:10.5194/acp-12-5259-2012.

Xie, S. P., K. Hu, J. Hefner, H. Tokinaga, Y. Du, G. Huang, and T. Sampe, 2009: Indian Ocean capacitor effect on Indo–western Pacific climate during the summer following El Niño. *J. Climate,* **22,** 730–747.

Xue, F., and C. Z. Liu, 2008: The influence of moderate ENSO on summer rainfall in eastern China and its comparison with strong ENSO (in Chinese). *Chin. Sci. Bull.,* **53,** 791–800, doi:10.1007/s11434-008-0002-5.

Yang, J., Q. Liu, S. P. Xie, Z. Liu, and L. Wu, 2007: Impact of the Indian Ocean SST basin mode on the Asian summer monsoon. *Geophys. Res. Lett.,* **34,** L02708, doi:10.1029/2006GL028571.

Yeh, S. W., J. S. Kug, B. Dewitte, M. H. Kwon, B. P. Kirtman, and F.-F. Jin, 2009: El Niño in a changing climate. *Nature,* **461,** 511–514, doi:10.1038/nature08316.

Yu, J. Y., and H.-Y. Kao, 2007: Decadal changes of ENSO persistence barrier in SST and ocean heat content indices: 1958–2001. *J. Geophys. Res.,* **112,** D13106, doi:10.1029/2006JD007654.

——, and S. T. Kim, 2010: Three evolution patterns of central-Pacific El Niño. *Geophys. Res. Lett.,* **37,** L08706, doi:10.1029/2010GL042810.

——, and ——, 2011: Relationships between extratropical sea level pressure variations and the central-Pacific and eastern-Pacific types of ENSO. *J. Climate,* **24,** 708–720.

——, C. R. Mechoso, J. C. McWilliams, and A. Arakawa, 2002: Impacts of the Indian Ocean on the ENSO cycle. *Geophys. Res. Lett.,* **29,** 1204, doi:10.1029/2001GL014098.

——, F. P. Sun, and H. Y. Kao, 2010: Subtropics-related interannual sea surface temperature variability in the central equatorial Pacific. *J. Climate,* **23,** 2869–2884.

——, H. Y. Kao, T. Lee, and S. T. Kim, 2011: Subsurface ocean temperature indices for central-Pacific and eastern-Pacific types of El Niño and La Niña events. *Theor. Appl. Climatol.,* **103,** 337–344, doi:10.1007/s00704-010-0307-6.

Zhang, R., A. Sumi, and M. Kimoto, 1996: Impacts of El Niño on the East Asian monsoon: A diagnostic study of the '86/87 and '91/92 events. *J. Meteor. Soc. Japan,* **74,** 49–62.

——, ——, and ——, 1999: A diagnostic study of the impact of El Niño on the precipitation in China. *Adv. Atmos. Sci.,* **16,** 229–241, doi:10.1007/BF02973084.

Zhang, W. J., F.-F. Jin, J. P. Li, and H.-L. Ren, 2011: Contrasting impacts of two-type El Niño over the western North Pacific during boreal autumn. *J. Meteor. Soc. Japan,* **89,** 563–569.

——, ——, H.-L. Ren, J. P. Li, and J. X. Zhao, 2012: Differences in teleconnection over the North Pacific and rainfall shift over the USA associated with two types of El Niño during boreal autumn. *J. Meteor. Soc. Japan,* **90,** 535–552.